ELSEVIER

Journal of Crystal Growth 237–239 (2002) 668–671

JOURNAL OF CRYSTAL GROWTH

www.elsevier.com/locate/jcrysgro

Morphologic characterization of $Dy_xY_{1-x}Al_3(BO_3)_4$ single crystals grown from the flux and vapour phase

R. Martínez Vázquez[a,*], M.A. Caballero[c], M. González-Mañas[c], E.P. Kokanyan[b], C.M. Ruiz[a], E. Diéguez[a]

[a] *Departamento de Física de Materiales, Universidad Autónoma de Madrid, 28049 Cantoblanco, Madrid, Spain*
[b] *Institute for Physical Research, National Academy of Sciences of Armenia, 375014 Yerevan, Armenia*
[c] *Departamento de Cristalografía y Mineralogía, Universidad de Cádiz, 11510 Pto. Real, Cádiz, Spain*

Abstract

$Dy_xY_{1-x}Al_3(BO_3)_4$ single crystals with different Dy concentrations from $x = 0.001$ to 0.1 have been grown from fluxed melts based on $K_2Mo_3O_{10}$–B_2O_3 mixtures, in the temperature range from 1070°C to 900°C. Platelets of Dy:YAB have been obtained by evaporation from the melt that clearly showed both growth sectors and striations. Bulk crystal has been grown from the melt by spontaneous crystallization with good optical quality.

Differential thermal analysis and X-ray diffraction have been used to study the behaviour of the initial mixed oxides, the growth conditions and the grown crystals. X-ray topography has been used to analyse the growth defects, the structure of the growth sectors and striations in the platelets.

PACS: 07.85.−m; 42.70.Mp; 61.10.−i

Keywords: A1. Nucleation; A1. X-ray diffraction; A1. X-ray topography; B1. Borates

1. Introduction

The alumino-borates with the chemical formula $YAl_3(BO_3)_4$ (YAB) have good thermal and chemical stability [1], and important applications in laser engineering [2]. Rare-earth doping has been investigated [3] as they are representative polyfunctional materials. The chemical and physical properties of their solid solutions and their single crystals have been extensively studied in the past [4,5].

The structure of YAB crystal is trigonal, isomorphous with huntite $CaMg_3(CO_3)_4$. The space group of YAB crystal is R32 with hexagonal lattice constants $a = 9.295(3)$ Å and $c = 7.243(2)$ Å [4].

Attending to laser properties most studies have been focused on Nd:YAB [6] as it has high efficiency because of its high non-linear coefficient, high threshold damage, good mechanical properties and high segregation coefficient for neodymium ions. In order to take advantage of these characteristics we have doped it with a new rare-earth ion: Dy^{3+}. Optical properties of this ion have been studied in other matrix like DyOCl [7], and potential laser emission has been proposed in a non-linear matrix like $Dy:GdCa_4O(BO_3)_3$ [8].

*Corresponding author. Tel.: +34-913-974-784; fax: +34-913-978-579.

E-mail address: rebeca.martinez@uam.es (R. Martínez Vázquez).

0022-0248/02/$ - see front matter
PII: S0022-0248(01)02053-X

The present work considers the system $Dy_xY_{1-x}Al_3(BO_3)_4$ from two points of view, one concerning the synthesis of this alumino-borate with x going from 0 to 1 and the other focused on the flux growth of this material with x ranging from 0.001 to 0.1. By X-ray powder analysis, the presence of a new reaction in the melt has been found. The formation and decomposition temperatures of this material are proposed. The goal of this paper is the illustration of the first stages of crystal growth, the identification of nucleation point and then to describe the external morphology of the crystals.

2. Experimental procedure

The powdered samples were synthesized from mixtures of the oxides B_2O_3, Dy_2O_3, Y_2O_3, Al_2O_3 by means of the solid-state reaction between them:

$$x\mathrm{Dy_2O_3} + (1-x)\mathrm{Y_2O_3} + 3\mathrm{Al_2O_3} + 4\mathrm{B_2O_3} \rightarrow 2\mathrm{Dy}_x\mathrm{Y}_{1-x}\mathrm{Al_3(BO_3)_4}. \quad (1)$$

The purity of the starting chemicals was as follows: Dy_2O_3 (99.99%), Y_2O_3 (99.999%), Al_2O_3 (99.995%), B_2O_3 (99.98%) and for flux synthesis ($K_2Mo_3O_{10}$), K_2CO_3 (99.997%) and MoO_3 (99.9995%).

For the study of powdered $Dy_xY_{1-x}Al_3(BO_3)_4$ (Dy:YAB) (from $x = 0$ to 1), the calculated amounts of these oxides were mixed, reground and pulled into pellets. These pellets were heated, in a SiC furnace, from RT to 1100°C and maintained there for 6 h, after this the pellets were thermally and compositionally analysed.

Single crystals of Dy:YAB (with $x = 0.001$, 0,05, 0.075 and 0.1) were obtained by spontaneous crystallization solution growth method, with $K_2Mo_3O_{10} + B_2O_3$ flux. The selection of flux and the starting composition of 20 wt% Dy:YAB, 75 wt% $K_2Mo_3O_{10}$ and 5 wt% B_2O_3 were chosen in accordance with previous studies on $Nd_xY_{1-x}Al_3(BO_3)_4$ growing [9]. The mixtures were kept in a Pt crucible covered with a Pt lid. The growing processes were carried out in an SiC furnace in the temperature range 1070–900°C with cooling rates of 0.4°C/h and 0.3°C/h.

From the same experiments Dy:YAB plates were obtained from melt evaporation and subsequent deposition on crucible walls.

Phase identifications of initial oxide mixtures, the materials obtained from synthesis and the residues of growth evaporation were taken from their X-ray powder diffraction (XRD) patterns. XRD measurements were carried out with a Siemens D5000 diffractometer using Cu K_α radiation and an Ni filter.

Thermal behaviour was investigated using a Perkin-Elmer DTA 1700. Charges of different pulverized pellets, initial oxides mixtures and pulverized crystals were studied in order to obtain the variation of decomposition temperature with the Dy content to compare with similar studies on Nd:YAB [10].

Crystals surface and plates were observed by optical microscope. After observing them, as-grown plates defects were investigated by X-ray topography. Transmission X-ray topographs were taken by a Lang method camera using Mo K_α radiation.

3. Results and discussion

It was found that evaporation during growth is principally composed of $K_2Mo_3O_{10}$ (JCPDS card No. 37-1467), $Al_{18}B_4O_{33}$ (JCPDS card No. 32-3), Al_3BO_6 (JCPDS cards No. 26-8, 32-4) as shown in Fig. 1. The presence of flux-related compound $K_2Mo_3O_{10}$ was expected because it is highly volatile [10]. $Al_{18}B_4O_{33}$ and Al_3BO_6 are supposed to belong to solid-state reactions in the melt, the presence of $Al_{18}B_4O_{33}$ has been found before [11] when studying the system $B_2O_3 + Y_2O_3 + Al_2O_3$. Al_3BO_6 compound may be related to the solid-state reaction (2) that could take place during the cooling process.

$$3\mathrm{Al_2O_3} + \mathrm{B_2O_3} \rightarrow 2\mathrm{Al_3BO_6}. \quad (2)$$

To study the decomposition temperature of Dy:YAB with Dy content, DTA was carried out from 900°C to 1350°C in nitrogen atmosphere. In this temperature range, there were two endothermic peaks for oxides mixtures and only one for the samples obtained in synthesis. The first peak appeared at 1146.7 ± 0.1°C and was identified as

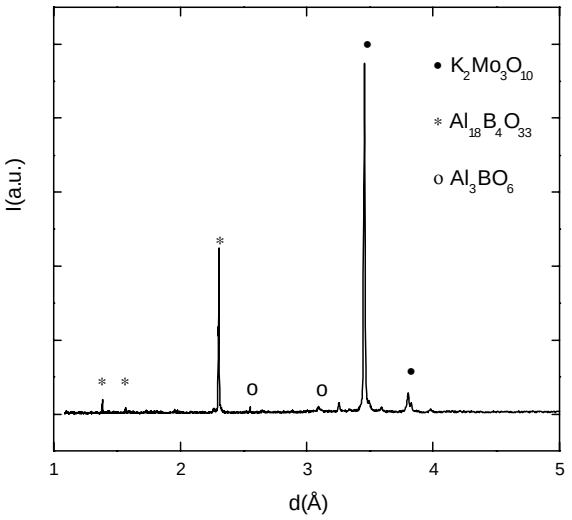

Fig. 1. X-ray powder diffraction spectra of the material deposited on crucible lid during a Dy:YAB flux growth.

Dy:YAB formation temperature, as it was not in synthesis analysis. The formation temperature did not show any dependence with the Dy content in contrast with the second peak identified as the decomposition temperature. As the Dy content was increased, the decomposition temperature decreased which is an evidence of the stronger interatomic forces with lower Dy^{3+} content. These temperatures range from 1276.2°C (for $x = 0.001$) to 1192.7°C (for $x = 1$). They are higher than the corresponding ones for Nd:YAB [10], as Dy^{3+} ionic radius is lower than Nd^{3+} more stability is expected for this new material.

The crystals obtained exhibited well-developed facets having the form of a prism and a rhombohedron (Fig. 2(a)), it is important to note that the face parallel to the picture is the rhombohedral plane $(1\,0\,\bar{1}\,1)$. There are some growth striations with polygonal structure parallel to crystal external faces and the longest direction of the crystal is the one perpendicular to the marked face (white circle) in Fig. 2(a). In the same crystal, there is a flux inclusion that could be an induced nucleation point. Comparing this picture with Fig. 2(b), where is shown the picture of one of the platelets, the similarity of growth striations in both crystals is evident, the plate is showing the first stages of the growth process.

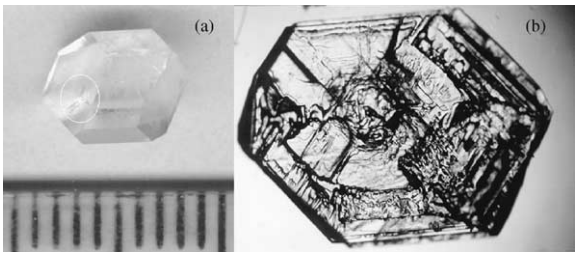

Fig. 2. Optical microscopy pictures of (a) a Dy:YAB crystal, there is a signal over growth striations; (b) a Dy:YAB plate, with a scale 1:40.

X-ray topographs of the plate in Fig. 2(b) are shown in Fig. 3, they were taken by the $1\,1\,\bar{2}\,0$ (a) and the $2\,0\,\bar{2}\,2$ (b) reflections, in (b) the high asymmetry factor is responsible for the flattened aspect of the plate. Different growth sectors (GS on the topographs) appear separated by the so-called growth sector boundaries (GSB on the topographs). The growth sectors are the pinacoidal $(0\,0\,1)$ in the central part of the crystal, the rhombohedric ones $\{1\,0\,\bar{1}\,1\}$ and a prismatic sector $(1\,1\,\bar{2}\,0)$ at the left of the crystal. The planar geometry of the GSB let us to conclude that the relative growth velocities of the adjacent growth sectors have not changed during the growth of the platelet. This planar geometry can be well observed in the topography in Fig. 3(b): two of these GSB show a contrast formed by two parallel lines in the intersection between GSB and crystal faces where the internal stress is relaxed. The GSB divide this crystal into regions of different orientation, as a consequence some of the regions, depending on the reflection used, are out of the exact Bragg position leading to less or no contrast at all. The misorientation measured is of the order of 300–400″ of arc.

The plate shows a great dislocation (D in the topographs) density, they appear in bundles in all the growth sectors. They are generated either in the GSB or in the flux inclusions (i in the topographs) trapped during growth, and they are propagated more or less perpendicular to the growth front. The dislocation also contributes to the distortion of certain zones of the crystal as can be clearly observed in the rhombohedric growth sector located in the upper part of the crystal (Fig. 3(a)). The topographs also show growth

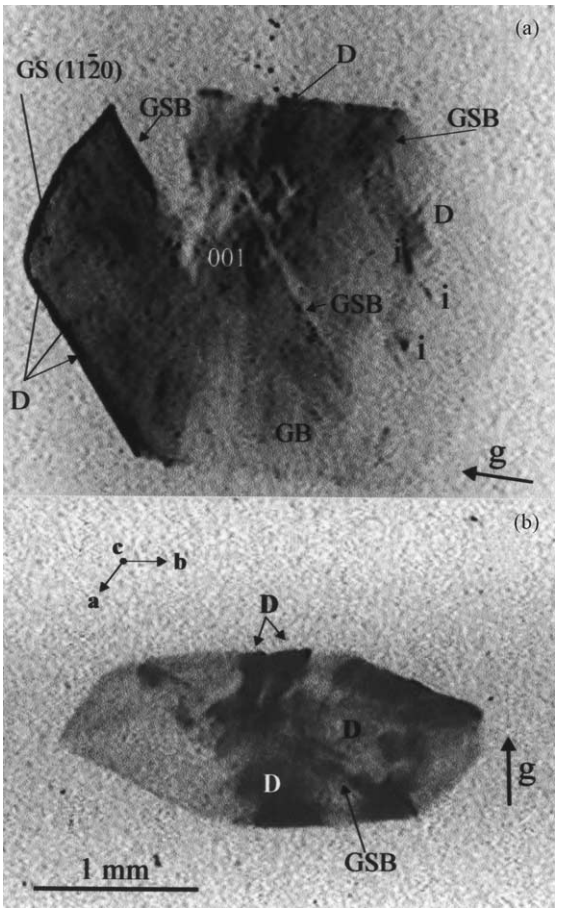

Fig. 3. X-ray topographs of the Dy:YAB plate: (a) (1 1 $\bar{2}$ 0)and (b) (2 0 $\bar{2}$ 2)reflections, respectively; GS: growth sector, GSB: growth sector boundaries, GB: growth striation, D: dislocations, i: inclusions.

striations (GB on the topographs) which are parallel to the external faces.

In view of these results, we can conclude that in the initial stages of the growth all the rhombohedral faces have the same probability of growth. This explains the morphology of the platelets. Then one of them will increase this growing velocity, and attending to all the single crystals obtained in this study, most times the (1 0 $\bar{1}$ 1) face is more developed leading to the high dimension in the direction perpendicular to this face. Looking to the top seeding solution growth of this material this can be the best seed orientation to increase its efficiency.

4. Conclusions

There are a lot of reactions in the melt during crystal growth some of them leading to the evaporation of products that condensate on crucible's lid, like Al_3BO_6. The evaporation of Dy:YAB also takes place, and in some cases its condensation on crucible walls develop new nucleation points.

The flux growth crystals show well-developed faces in their external morphology. At the first stages of crystal growth most faces have the same growth velocity and at cooler temperatures one of them increases its growth velocity and this will lead to the higher dimension of the crystal.

Acknowledgements

One of the authors (R.M.V.) thanks the Vicerrectorado de Investigación of UAM for a fellowship. This work has been partially supported by CAM Project 07T/0042/2000.

References

[1] E.V. Koporulina, N.I. Leonyuk, S.N. Barilo, L.A. Kurnevich, G.L. Bychkov, A.V. Mokhov, G. Bocelli, L. Righi, J. Crystal Growth 198/199 (1999) 460.
[2] J.T. Lin, Laser Optron. 34 (1990).
[3] E.V. Koporulina, N.I. Leonyuk, D. Hansen, K.L. Bray, J. Crystal Growth 191 (1998) 767.
[4] N.I. Leonyuk, L.I. Leonyuk, Prog. Crystal Growth Charact. 31 (1995) 179.
[5] N.I. Leonyuk, Prog. Crystal Growth Charact. 31 (1995) 279.
[6] D. Jaque, J. Capmany, J. García Solé, Z.D. Luo, A.D. Jiang, J. Opt. Soc. Am. B. 15 (1998) 6.
[7] J. Hölsä, R.-J. Lamminmäki, P. Porcher, P. Derán, W. Strek, Spectrochim. Acta Part A 54 (1998) 398.
[8] S. Zhang, Z. Cheng, Z. Zhuo, J. Hen, H. Chen, Phys. Stat. Sol. A 181 (2000) 485.
[9] N.I. Leonyuk, E.V. Koporulina, S.N. Barilo, L.A. Kurnevich, G.L. Bychkov, J. Crystal Growth 191 (1998) 135.
[10] S.T. Jung, D.Y. Choi, S.J. Chung, Mater. Res. Bull. 31 (1996) 8.
[11] E. Beregui, A. Watterich, L. Koudes, J. Madarász, Vibrational Spectrosc. 22 (2000) 169.